

Spin configuration of 4T_1 and 6A_1 states in a manganese-doped wide band gap semiconductor

Sourav Mukherjee,¹ Soirik Dan,^{1,*} Biswajit Kundu,^{1,*} and Amlan J. Pal^{1,2,†}

¹*School of Physical Sciences, Indian Association for the Cultivation of Science, Jadavpur, Kolkata 700032, India*

²*UGC-DAE Consortium for Scientific Research, University Campus, Khandwa Road, Indore 452001, India*



(Received 24 December 2022; revised 8 February 2023; accepted 15 February 2023; published 24 February 2023)

We probe the spin configuration of manganese's d states, namely 4T_1 and 6A_1 , in doped semiconductor quantum dots (QDs) through spin-polarized scanning tunneling spectroscopy (SP-STs). We show that the two levels have opposing spin states. Experimentally, we probed the density of states (DOS) of the undoped and manganese-doped ZnS QDs, which have a wide band gap so that the 4T_1 and 6A_1 energies lie within the gap. The states were viewed with a nonmagnetic and a spin-polarized tip of a scanning tunneling microscope (STM). While a nonmagnetic tip could inject electrons into the 4T_1 and withdraw electrons from the 6A_1 state as well, the DOS derived with a spin-polarized tip evidenced that the tip could “see” only one of the two energy levels, whose spin state remained parallel to that of the tip. The intensity of DOS representing the 4T_1 and 6A_1 of manganese thereby depended on the mutual alignment of the magnetization vectors representing the tip and the d states. We have inferred that the spin configuration of 4T_1 and 6A_1 states is mutually antiparallel in nature; such results have been the rationale of the photoluminescence (PL) emission in such manganese-doped QDs to possess an exceptionally long lifetime.

DOI: [10.1103/PhysRevB.107.075434](https://doi.org/10.1103/PhysRevB.107.075434)

I. INTRODUCTION

Diluted magnetic semiconductors (DMSs) are continuing to receive a lot of attention in the field of condensed matter physics and applied physics due to their prospective applications in spintronic and optoelectronic devices [1–5]. Some traditional compound semiconductors, when doped with a suitable transition metal, may possess important optical, electrical, magnetic, and spintronic properties [6–9]. One of the well-studied and prototype DMS materials has been manganese-doped ZnS, in which manganese (Mn) is added to the structure of the II-VI semiconductor. Accordingly, Mn-doped ZnS, often in their lower-dimensional forms, is used in a variety of applications, such as lighting devices, light-emitting diodes, solar cells, sensors, infrared windows, biodevices, ceramics, photocatalysis, and magnetoelectronics, due to their lower toxicity, larger Stokes shifts, and improved thermal and environmental stability [10–13]. More importantly, due to the wide band gap of the host chalcogenide, the characteristic energy levels of manganese, namely 4T_1 and 6A_1 , lie clearly within the band gap and prompt interesting optical properties. Such a unique combination of the host's band edges and dopant's energy levels yields a yellow-orange signature emission with a low full width at half maximum (FWHM); the photoluminescence (PL) emission of manganese-doped semiconductors has an uncharacteristically long decay lifetime [5,14,15].

Manganese impurities have been known to give rise to the characteristic yellow-orange emission in wide band gap ma-

terials indicating a ${}^4T_1 \rightarrow {}^6A_1$ transition, which has been the subject of extensive research in quantum dots (QDs) as well as in bulk semiconductors [15–21]. The magnetic component exhibits exchange interactions with band-edge carriers in a variety of semiconductor hosts. Hence, nonmagnetic semiconductors, when doped with magnetic ions like transition metals and rare-earth metals, are considered to be ideal candidates for spintronic applications, since the dopants embed multiple functions in terms of both the spin and the charge of electrons [22,23]. In other words, the interaction between unpaired d electrons of the transition metal and the bands of the host material leads to a number of interesting spintronic properties. The Mn-doped semiconductors are thereby being extensively explored in order to investigate and comprehend their emission properties [24].

While a lot of efforts have been dedicated to studying the structural and electronic properties of the DMSs often in their lower dimensional forms, their spintronic aspect has remained interesting over the years. In this direction, the pump-probe method has mostly been employed to measure spin dynamics, such as spin relaxation time. The optical approach however remained somewhat incomplete in revealing the spin states of manganese in the quantum dot (QD) form of the doped semiconductors [25,26]. In spin-polarized scanning tunneling microscopy and spectroscopy (SP-STM/S), tunneling of spin-polarized electrons by the spin-polarized tip to the semiconductor surface (or from the semiconductor surface to the tip) will occur. The spectroscopy will hence sense the spin state(s) of the semiconductor's energy levels and thereby can be an effective technique to probe the surface magnetism with an atomic-scale spatial resolution. In this work, we thereby employed SP-STs to probe the spin states and electronic states of manganese's d levels in a wide band gap semiconductor,

*These authors contributed equally to this work.

†sspajp@iacs.res.in

since the spin-polarized electrons of the spin-polarized STM tip may “see” the spin states of the energy levels while tunneling to/from them.

II. EXPERIMENTAL SECTION

A. Materials

Zinc stearate, $\text{Zn}(\text{St})_2$, octadecylamine (ODA, 97%), octadecene (ODE, 90%), stearic acid (95%), manganese chloride (MnCl_2 , 99%), tetramethylammonium hydroxide (TMAH, 25 wt % in water), and sulfur powder (99.98%) were procured from Sigma Aldrich Chemical Company. Au (111) substrates used for STS measurements were purchased from M/s Phasis Sàrl, Switzerland. All the materials were used without further purification.

B. Synthesis of manganese stearate, $\text{Mn}(\text{St})_2$

Manganese stearate was synthesized following a colloidal synthesis process for the preparation of Mn-doped ZnS. First, 2.84 g stearic acid was dissolved in 20 mL of methanol through stirring and heating to 50–60 °C until a clear solution was formed. 10 mmol (0.91 mL) of TMAH dissolved in 6 mL of methanol was then added to the stearic acid solution, which was further stirred for 15 min. In the following step, MnCl_2 (989.5 mg) dissolved in 6 mL methanol in a separate vial was added dropwise to the reaction flask under a vigorous stirring condition resulting in a steady flocculation of $\text{Mn}(\text{St})_2$ in the form of a white precipitate. The precipitate was washed several times in methanol to remove unreacted components and then put in a desiccator under vacuum for drying.

C. Synthesis of QDs

To grow ZnS QDs through a well-established method, $\text{Zn}(\text{St})_2$ stock solution was first prepared by dissolving 0.63 g of ZnSt_2 and 0.284 g of stearic acid in 4 mL of ODE in a vial under an inert environment. To initiate the reaction process, 0.063 g of $\text{Zn}(\text{St})_2$ and 0.016 g of sulfur powder were put in a 50-mL three-necked round-bottom reaction flask, in which 0.8 g of ODA and 10 mL of ODE were added. The flask was fitted with a reflux condenser. To form Mn-doped ZnS QDs, 3 mg of $\text{Mn}(\text{St})_2$ was also added to the reaction mixture; the achieved concentration of manganese in the QDs was 2.8%. The solution mixture was put into an inert atmosphere by purging nitrogen; the temperature of the flask was then raised to 270 °C. After 5 min, the temperature was reduced to 250 °C and the as-prepared ZnSt_2 stock solution was injected into the reaction mixture. The reaction process was allowed to continue for 30 min without any disturbance. After the flask was cooled down to room temperature, the synthesized QDs were dispersed in hexane and the solution was repeatedly centrifuged at 3000 rpm until a clear solution could be witnessed. The synthesized QDs were used for further experiments.

D. Characterization of QDs

The optical properties of undoped and Mn-doped ZnS QDs in dispersed solutions of hexane were characterized through UV-visible optical absorption and PL spectroscopy using a Shimadzu UV-2550 spectrophotometer and a Horiba

Jobin Yvon Fluoromax-4 spectrofluorometer, respectively. The excitation wavelength for the emission spectroscopy measurements was 320 nm. The structural properties of the QDs, including crystal structure and size, were determined using x-ray diffraction (XRD) patterns obtained from a Bruker D8 advanced x-ray powder diffractometer with $\text{Cu } K_\alpha$ ($\lambda = 1.54 \text{ \AA}$) as an incident radiation. The QDs were also characterized for high-resolution transmission electron microscopy (HR-TEM) and x-ray photoelectron spectroscopy (XPS) using JEM-2100F Jeol microscope operated at 200 kV and Omicron (serial number 0571) electrospectrometer systems, respectively. Additionally, energy-dispersive x-ray (EDX) analysis yielded the elemental analysis of the synthesized QDs.

Ultrahigh vacuum scanning tunneling microscopy (UHV-STM) of the QDs was recorded by using a PAN-style UHV-STM (M/s RHK Technologies, Troy, MI), in which the tip and the substrate attain the same temperature. During the measurements, the temperature of the cryostat was maintained at 80 K while the base pressure of the microscope chamber was 7.2×10^{-10} Torr. The substrate electrodes for the measurements were 100-nm-thick gold-coated mica. The undoped and Mn-doped ZnS QDs were deposited on the electrode substrates through a drop-cast method from their dilute solutions. Topography and spectroscopy of the QDs were recorded with extremely sharp STM tips formed through an acute mechanical cut of a Pt/Ir (80%/20%) wire which had a diameter of 0.25 mm. For SP-STs measurements, a chromium-coated antiferromagnetic tip, purchased from NaugaNeedles LLC was used; such tips, with the magnetization direction along the axis, allowed injection or withdrawal of spin-polarized electrons. For the approach of the tip, a bias of 2.0 V was used to achieve a set current of 200 pA through a feedback loop. To record the dI/dV versus voltage characteristics, a lock-in amplifier (18 mV rms, 973 Hz) was used.

III. RESULTS AND DISCUSSION

Before probing the ZnS and Mn-doped ZnS QDs through STS and SP-STs, we characterized the QDs for their optical and structural properties; such characteristics have been discussed and presented in Figs. S1–S4 in the Supplemental Material [27] and references therein [5,6,14,16–20,28]. It is well reported that the PL emission of the doped QDs originated upon an energy transfer to the d state of manganese from the band edge of the host followed by a radiative transition between the 4T_1 and 6A_1 states of Mn^{2+} [18,28]. The yellow-orange emission is generally associated with a long decay lifetime (on the order of millisecond) implying the transition to possess a spin-forbidden character [5,14]; the PL emission of the undoped QDs appearing from the host semiconductor, however, had a short lifetime [5]. Decay characteristics of the undoped and manganese-doped ZnS QDs have been presented in Fig. S5 in the Supplemental Material [27]. The results matched quite well with the reported literature [5].

We then recorded the energy-dependent density of states (DOS) of the QDs through a STM tip under an UHV condition. A typical large-scale STM topography recorded in a constant-current mode is shown in Fig. S6 in the Supplemental Material [27]. We first used a Pt/Ir tip to record differential

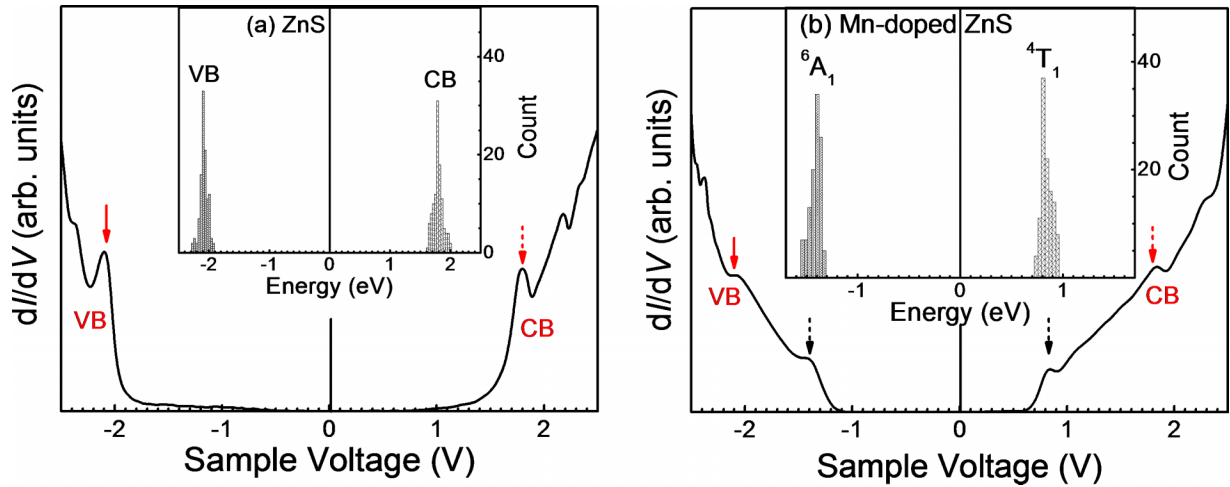


FIG. 1. A typical dI/dV spectrum of (a) undoped and (b) Mn-doped ZnS QDs recorded with a Pt/Ir tip. Insets show histogram of CB and VB energies with respect to the Fermi level.

tunnel conductance (dI/dV) as a function of voltage which was applied to the substrate electrode. The dI/dV spectra in turn have provided energy-dependent DOS of the materials. The differential tunnel conductance (dI/dV) can be expressed as [29]

$$\frac{dI}{dV} \propto |M|^2 p_T(E_F) p_S(E_F), \quad (1)$$

where p_T and p_S are the DOS of the tip and the sample, respectively, and M stands for the tunneling matrix element. Since the dI/dV has a correspondence to the DOS of the semiconductor, the first peak in the positive voltage of a dI/dV spectrum implied the injection of electrons to the conduction band (CB). Likewise, the first peak in the negative bias region implied the withdrawal of electrons and thereby the location of the valence band (VB). In Fig. 1(a), we present a typical dI/dV spectrum of an undoped ZnS QD on a gold substrate. The spectrum provided the energy of the CB and the VB with respect to the Fermi level, which is aligned to 0 V in STS measurements, in the form of a peak in the positive and the negative voltage region, respectively. Since STS is an extremely localized mode of measurement, we recorded many spectra on a QD and also on many QDs having quite similar diameters. As the transport gap and thereby the band edges would depend on the diameter of the QD, we had to target the QDs that have a mostly identical diameter (2.9 nm). We located the band energies from each dI/dV spectrum and collated them in the form of a histogram in obtaining a macroscopic view [inset of Fig. 1(a)]. While the width of the histograms appeared due to some variation in the QDs' diameters and defects present in the QDs, the peak provided the CB and VB energies of the undoped ZnS QDs. The transport gap turned out to be 3.9 eV which is a little higher than the optical band gap; such behavior is expected due to the involvement of the exciton binding energy in the optical band gap. The histogram of energies presented in Fig. 1(a) furthermore shows that the CB edge was closer to the Fermi level as compared to the VB energy. Such an observation implies that the QDs had an n -type character, which is known

to appear in the colloidal synthesis route due to the formation of sulfur vacancies.

We then proceeded to record STS of the Mn-doped ZnS QDs in a similar manner. Since the d states of manganese would also participate in the electron tunneling process, their presence within the band gap can be probed energetically and investigated in STS. In Fig. 1(b), we have presented a typical spectrum. Apart from the peaks representing the CB and the VB edges [which matched the edges observed in the undoped QDs and presented in Fig. 1(a)], the spectrum provided a couple of peaks within the band gap: one below the CB and one above the VB. These additional peaks in the dI/dV spectrum in fact represented the energies of the 4T_1 and 6A_1 states, respectively, since their difference matched the energy of PL emission observed from Mn-doped ZnS QDs. That is, the STS measurements could probe the CB and VB edges of the host QD and the d states of the manganese-dopant as well. We naturally recorded STS on many different QDs having similar diameters to collate the energies of the 4T_1 and 6A_1 states and also of the CB and VB edges of the host matrix. In the inset of Fig. 1(b), we have presented the histogram of energies representing the 4T_1 and 6A_1 states; we did not add the histograms of the CB and VB energies for clarity and their similarity with that obtained from the undoped QDs [inset of Fig. 1(a)]. The peaks in the histogram provided the energies of the two states of manganese. The histograms have a much lower FWHM as compared to the FWHM of the CB and VB energies for the undoped and also the doped QDs, since neither the diameter of the QDs nor the defects would affect the energies of the 4T_1 and 6A_1 states.

We also studied the effect of diameter variation of ZnS QDs and Mn-doped ZnS QDs on the dI/dV spectra (Fig. 2). When QDs with a smaller diameter were probed, the band edges moved away from the Fermi level. The nature of conductivity remained n type and did not depend on the diameter of the QDs. The transport gap of both undoped and Mn-doped ZnS QDs thereby responded to the diameter in the usual manner considering the quantum confinement effect. When doped QDs with a larger or a smaller diameter were selected, the energy of the d states remained unaltered while the CB and

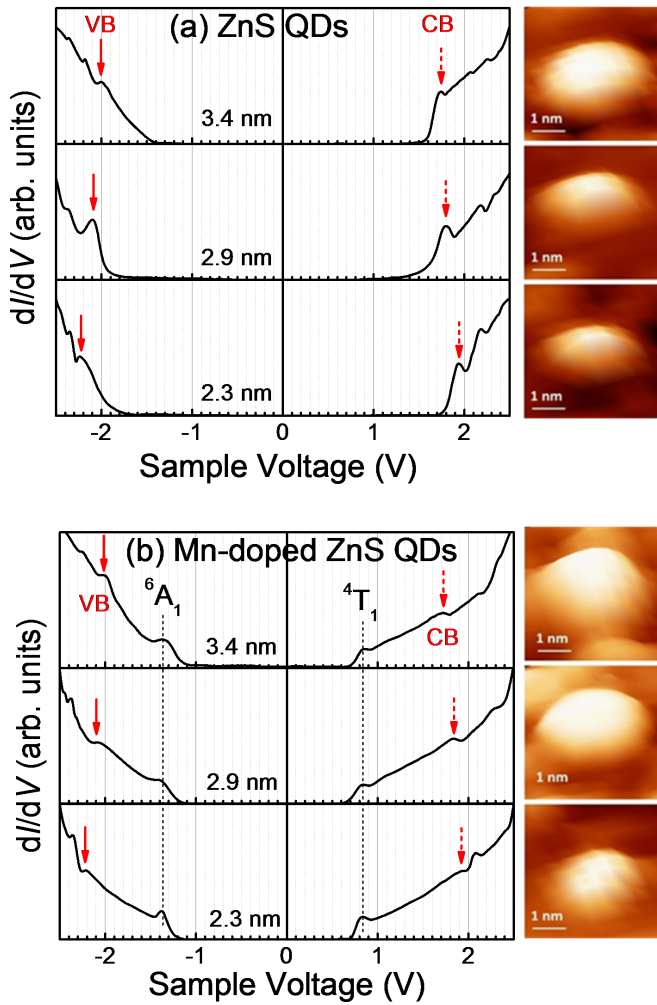


FIG. 2. dI/dV spectra of (a) undoped and (b) Mn-doped ZnS QDs for three different diameters recorded with a Pt/Ir tip. STM topographies of the respective QDs are shown on the right of each spectrum.

VB edges expectedly depended on the diameter. Since the energies of the d states do not depend on the band edges of the host matrix, the energies representing the 4T_1 and 6A_1 states did not respond to the diameter of the QDs. The invariance has been the rationale for the yellow-orange PL emission in Mn-doped QDs with a short FWHM.

Since the STS measurements could sense the d -state energies of manganese in the wide band gap doped QDs, SP-STs studies can be utilized to probe their spin states as well. According to Wortmann *et al.* [30], the spin-resolved differential tunneling conductance dI/dV can be expressed as a sum of the spin-averaged and the spin-polarized contribution, dI/dV_{SA} and dI/dV_{SP} , respectively [31]:

$$\frac{dI}{dV}(\mathbf{r}_t, V) \propto \mathbf{n}_t \cdot \mathbf{n}_s(\mathbf{r}_t, eV) + \mathbf{m}_t \cdot \mathbf{m}_s(\mathbf{r}_t, eV), \quad (2)$$

where \mathbf{n}_t and \mathbf{m}_t are the spin-averaged and magnetic tip's density of states, respectively, and \mathbf{n}_s and \mathbf{m}_s are the sample properties at the tip position \mathbf{r}_t . The first term on the right side represents dI/dV_{SA} , while the second term represents dI/dV_{SP} . A magnetic sample for SP-STM, on the other hand,

must meet the following requirements in order to be probed for: (i) it must be binary, with one of the two atom types being magnetic, (ii) magnetic moments must be primarily localized on magnetic atoms, and (iii) a significant number of spin-polarized states must exist in close proximity to the Fermi level (E_F). The spin-polarized d band is typically close to the Fermi surface in binary transition metal complexes. The spin orientation of the tunneling electrons is expected to remain constant during the tunneling process, implying that the spin-up electrons will always tunnel into a spin-up state and spin-down electrons will tunnel into a spin-down state. When materials with a particular spin polarization are used for the tip and the sample, the tunneling current is thus determined by the spin-dependent electrical properties of both electrodes.

We thereby repeated the measurements in the two types of QDs with a spin-polarized STM tip. Throughout the measurement, temperature of the tip-sample system was maintained far below the Néel temperature of the antiferromagnetic tip, which thereby did not affect the magnetic stability of the QDs. That is, due to the antiferromagnetic nature of the tip, the apex of the tip did not influence the spin state of the levels being probed. Since the tip would now inject (or withdraw) only one type of spin-polarized electrons, the tunneling process would require a match in the spin states of the SP-STM tip and the energy level involved in the electron tunneling process. The dI/dV spectra of undoped QDs recorded with a spin-polarized tip resembled the spectrum with a Pt/Ir tip, since the CB and VB energies did not expectedly depend on the configuration of magnetization vectors at the tip. When we recorded dI/dV spectra with a spin-polarized tip on many Mn-doped QDs, we obtained two types of spectra. In the upper and lower panels of Fig. 3(a), we have presented one each typical spectrum from the two groups. When they are compared with the spectrum of Mn-doped ZnS QDs recorded with a Pt/Ir tip (placed in the middle panel for comparison), we find that out of the two energies representing the manganese's d states, either 4T_1 or 6A_1 appeared in the form of a peak within the band gap; both the states never appeared in a single spectrum recorded with a spin-polarized tip. The energies matched the d states of manganese obtained in the dI/dV spectra recorded with a Pt/Ir tip [Fig. 3(a): middle panel]. Their difference thereby matched the energy of the PL emission. The CB and VB edge of the host QD could be seen to appear as peaks in both spectra. The results presented in Fig. 3 not only are intriguing but also contain rich physics and need detailed discussion.

Since we have recorded dI/dV spectra with a spin-polarized tip on many points of an Mn-doped QD and also on many such QDs, the selection of QDs bearing identical diameters was not necessary here. In the form of box plots [Fig. 3(b)], we have placed the energies and the DOS intensities representing the 4T_1 and 6A_1 states observed in Fig. 3(a) with the respective experimental conditions. The plots clearly show that the DOS intensity of only one of the two states (either 4T_1 or 6A_1) was clearly high in the two types of spectra. Both the 4T_1 or 6A_1 states never appeared in a single spectrum recorded with a spin-polarized tip. In measurements with a nonmagnetic tip, the DOS intensities of the two levels remained similar (middle panel). The energies of 4T_1 or 6A_1

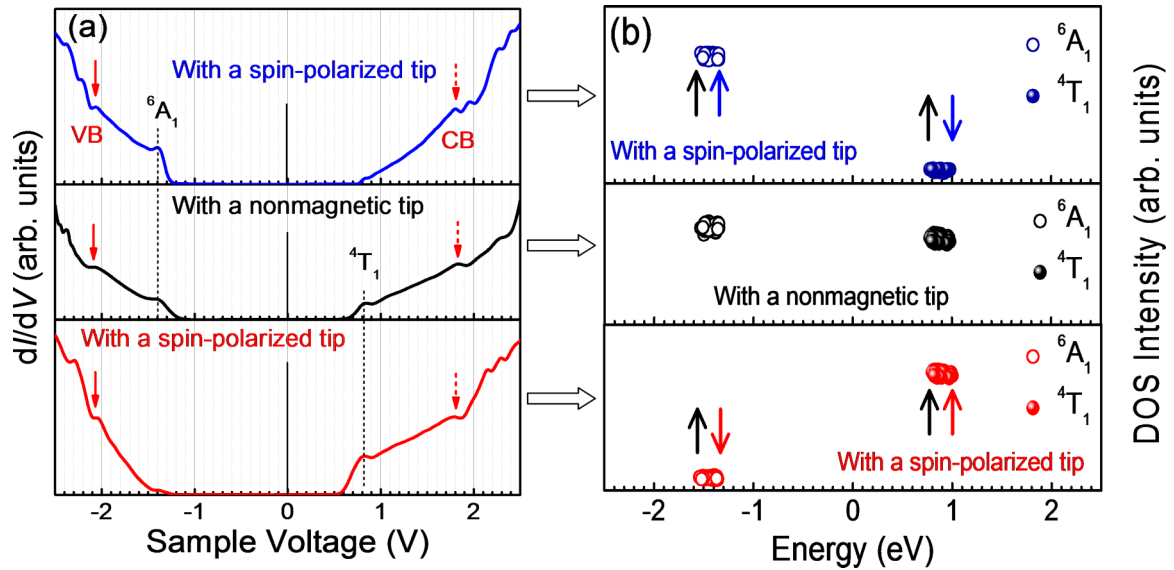


FIG. 3. (a) Two types of dI/dV spectra recorded with a spin-polarized tip of Mn-doped ZnS QDs (upper and lower panels). In the middle panel, a dI/dV spectrum of the QDs recorded with a Pt/Ir tip is replotted to make a comparison. (b) Box plots of the DOS energies and intensities representing the 4T_1 and/or 6A_1 states observed in the three corresponding measurements.

levels naturally did not depend on the spin character of the tip used in recording the tunneling characteristics.

The results presented in Fig. 3 implied that the DOS of the d states (4T_1 and 6A_1) recorded with an SP-STM tip depended on the relative alignment of the spin state of the tip and of the manganese's d states. Their relative alignment can be either parallel or antiparallel. The plots demonstrate that the DOS is influenced by the mutual alignment of the magnetization vectors; a peak appears in the DOS only when the spin magnetization vectors of the tip and of the d state(s) are parallel to each other. In other words, when the magnetization vectors of the tip and the particular d state are parallel, spin-polarized electrons may “see” a greater number of available states into (from) which the electrons can be injected (withdrawn). In contrast, the spin-polarized tip detects a low DOS intensity in the d state to inject or withdraw spin-polarized electrons when they are in an antiparallel configuration. The upper panels of Figs. 3(a) and 3(b) show that the manganese's 6A_1 state is more prominent as compared to the 4T_1 state, implying that the spin-magnetization vectors of the tip and 6A_1 were parallel to each other. The lower panels of the figures, on the other hand, show that the 4T_1 state is more prominent, implying that the spin-magnetization vectors of the tip and the 6A_1 are in antiparallel configuration. Only one of the two states (either 4T_1 or 6A_1) thereby appeared in the spin-polarized spectra. The results hence establish the overall spin asymmetries of the two d states that manganese possesses. That is, the 6A_1 and 4T_1 states of manganese have opposing spin configurations.

The two possible spin configurations of the 4T_1 and 6A_1 states along with the transition involved in the system have been presented schematically in Fig. 4. The results are hence direct evidence of the spin-forbidden nature of the $^4T_1 \rightarrow ^6A_1$ transition in Mn-doped QDs; since the PL appears due

to the transition, the emission has a long lifetime as compared to the PL emission from the host matrix (Fig. S5 in the Supplemental Material [27]). The aforementioned findings demonstrate that the intensity modulated DOS is the distinctive feature used to identify spin-dependent signals in SP-STs studies. It may be touched upon that the energy of the 4T_1 state when probed with a spin-polarized tip was a little farther from the Fermi level as compared to the energy obtained with a nonmagnetic tip. For the 6A_1 state, the energies matched very well. This may have occurred due to a strong ferromagnetic coupling of the 4T_1 state.

IV. CONCLUSION

In conclusion, we have probed the relative spin configuration of 4T_1 and 6A_1 states in a manganese-doped

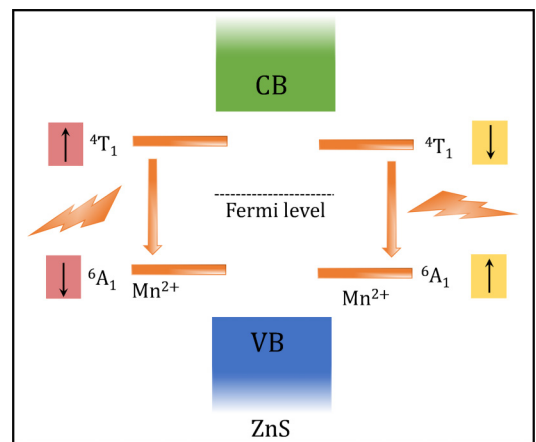


FIG. 4. A schematic representation of the spin configurations in 4T_1 and 6A_1 states in Mn-doped ZnS QDs.

semiconductor quantum dot system with the aid of spin-polarized STS. Since the spin states of the tip should be aligned to the d state(s) in achieving an effective electron-tunneling process, the DOS intensity became a measure of the two states' relative spin configuration. In STS recorded with a spin-polarized tip, either the 4T_1 or the 6A_1 state could be seen as a peak in the DOS spectra; both states never appeared in a single DOS spectrum. In measurements with a nonmagnetic tip, both levels were manifested with an equal DOS intensity. We accordingly have concluded that the 4T_1 or 6A_1 states possess opposing spin configurations. Since the PL in Mn-doped QDs originates due to a ${}^4T_1 \rightarrow {}^6A_1$ transition, the results are hence a direct experimental explanation of a long decay

time of the PL emission in manganese-doped semiconductor quantum dots; that is, the decay time has been long due to the spin-forbidden nature of the transition between the d states.

ACKNOWLEDGMENTS

A.J.P. acknowledges a JC Bose National Fellowship of SERB (Grant No. JBR/2021/000001) and the Asian Office of Aerospace Research and Development (AOARD) from Grant No. FA2386-21-1-4031. S.M. and S.D. acknowledge DST-INSPIRE (IF 210231) and a UGC Fellowship (ID No. 191620026897), respectively.

The authors declare no conflict of interest.

-
- [1] D. J. Norris, N. Yao, F. T. Charnock, and T. A. Kennedy, High-quality manganese-doped ZnSe nanocrystals, *Nano Lett.* **1**, 3 (2001).
- [2] S. C. Erwin, L. J. Zu, M. I. Haftel, A. L. Efros, T. A. Kennedy, and D. J. Norris, Doping semiconductor nanocrystals, *Nature (London)* **436**, 91 (2005).
- [3] J. Z. Liu, P. X. Yan, G. H. Yue, J. B. Chang, D. M. Qu, and R. F. Zhuo, Red light photoluminescence emission from Mn and Cd Co-doped ZnS one-dimensional nanostructures, *J. Phys. D: Appl. Phys.* **39**, 2352 (2006).
- [4] D. J. Norris, A. L. Efros, and S. C. Erwin, *Doped nanocrystals*, *Science* **319**, 1776 (2008).
- [5] Z. Deng, L. Tong, M. Flores, S. Lin, J.-X. Cheng, H. Yan, and Y. Liu, High-quality manganese-doped zinc sulfide quantum rods with tunable dual-color and multiphoton emissions, *J. Am. Chem. Soc.* **133**, 5389 (2011).
- [6] S. Biswas, S. Kar, and S. Chaudhuri, Optical and magnetic properties of manganese-incorporated zinc sulfide nanorods synthesized by a solvothermal process, *J. Phys. Chem. B* **109**, 17526 (2005).
- [7] R. Beaulac, P. I. Archer, S. T. Ochsenein, and D. R. Gamelin, Mn^{2+} -Doped CdSe quantum dots: New inorganic materials for spin-electronics and spin-photonics, *Adv. Funct. Mater.* **18**, 3873 (2008).
- [8] A. Sahu, M. S. Kang, A. Kompch, C. Notthoff, A. W. Wills, D. Deng, M. Winterer, C. D. Frisbie, and D. J. Norris, Electronic impurity doping in CdSe nanocrystals, *Nano Lett.* **12**, 2587 (2012).
- [9] L. W. Dai, C. Strelow, T. Kipp, A. Mews, I. Benkenstein, D. Eifler, T. H. Vuong, J. Rabeah, J. McGettrick, R. Lesyuk, and C. Klinke, Colloidal manganese-doped ZnS nanoplatelets and their optical properties, *Chem. Mater.* **33**, 275 (2021).
- [10] M. L. Steigerwald and L. E. Brus, Semiconductor crystallites - A class of large molecules, *Accounts Chem. Res.* **23**, 183 (1990).
- [11] A. Henglein, P. Mulvaney, and T. Linnert, Chemistry of silver aggregates in aqueous-solution - nonmetallic oligomers and metallic particles, *Electrochim. Acta* **36**, 1743 (1991).
- [12] A. A. Khosravi, M. Kundu, B. A. Kuruvilla, G. S. Shekhawat, R. P. Gupta, A. K. Sharma, P. D. Vyas, and S. K. Kulkarni, Manganese-doped zinc-sulfide nanoparticles by aqueous method, *Appl. Phys. Lett.* **67**, 2506 (1995).
- [13] P. Reiss, J. Bleuse, and A. Pron, Highly luminescent CdSe/ZnSe Core/Shell nanocrystals of low size dispersion, *Nano Lett.* **2**, 781 (2002).
- [14] R. N. Bhargava, D. Gallagher, X. Hong, and A. Nurmikko, Optical-Properties of Manganese-Doped Nanocrystals of ZnS, *Phys. Rev. Lett.* **72**, 416 (1994).
- [15] L. R. Bradshaw, J. W. May, J. L. Dempsey, X. S. Li, and D. R. Gamelin, Ferromagnetic excited-state Mn^{2+} dimers in $Zn_{1-x}Mn_xSe$ quantum dots observed by time-resolved magnetophotoluminescence, *Phys. Rev. B* **89**, 115312 (2014).
- [16] N. Karar, F. Singh, and B. R. Mehta, Structure and photoluminescence studies on ZnS : Mn nanoparticles, *J. Appl. Phys.* **95**, 656 (2004).
- [17] D. Son, D. R. Jung, J. Kim, T. Moon, C. Kim, and B. Park, Synthesis and photoluminescence of Mn-doped zinc sulfide nanoparticles, *Appl. Phys. Lett.* **90**, 101910 (2007).
- [18] B. B. Srivastava, S. Jana, N. S. Karan, S. Paria, N. R. Jana, D. D. Sarma, and N. Pradhan, Highly luminescent Mn-doped ZnS nanocrystals: Gram-scale synthesis, *J. Phys. Chem. Lett.* **1**, 1454 (2010).
- [19] A. K. Kole and P. Kumbhakar, Effect of manganese doping on the photoluminescence characteristics of chemically synthesized zinc sulfide nanoparticles, *Appl. Nanosci.* **2**, 15 (2012).
- [20] R. K. Chandrakar, R. N. Baghel, V. K. Chandra, and B. P. Chandra, Synthesis, characterization and photoluminescence studies of Mn doped ZnS nanoparticles, *Superlattices Microstruct.* **86**, 256 (2015).
- [21] X. L. Yang, C. D. Pu, H. Y. Qin, S. J. Liu, Z. A. Xu, and X. G. Peng, Temperature- and Mn^{2+} concentration-dependent emission properties of Mn^{2+} -doped ZnSe nanocrystals, *J. Am. Chem. Soc.* **141**, 2288 (2019).
- [22] J. K. Furdyna, Diluted Magnetic semiconductors, *J. Appl. Phys.* **64**, R29 (1988).
- [23] H. Saadaoui, X. Luo, Z. Salman, X. Y. Cui, N. N. Bao, P. Bao, R. K. Zheng, L. T. Tseng, Y. H. Du, T. Prokscha, A. Suter, T. Liu, Y. R. Wang, S. Li, J. Ding, S. P. Ringer, E. Morenzoni, and J. B. Yi, Intrinsic Ferromagnetism in the Diluted Magnetic Semiconductor Co:TiO₂, *Phys. Rev. Lett.* **117**, 227202 (2016).
- [24] A. Hazarika, A. Pandey, and D. D. Sarma, Rainbow emission from an atomic transition in doped quantum dots, *J. Phys. Chem. Lett.* **5**, 2208 (2014).
- [25] G. Costantini, A. Rastelli, C. Manzano, P. Acosta-Diaz, R. Songmuang, G. Katsaros, O. G. Schmidt, and K. Kern, Inter-

- play between Thermodynamics and Kinetics in the Capping of InAs/GaAs(001) Quantum Dots, *Phys. Rev. Lett.* **96**, 226106 (2006).
- [26] J. M. Ripalda, D. Granados, Y. Gonzalez, A. M. Sanchez, S. I. Molina, and J. M. Garcia, Room Temperature emission at 1.6 μm from InGaAs quantum dots capped with GaAsSb, *Appl. Phys. Lett.* **87**, 202108 (2005).
- [27] See Supplemental Material at <http://link.aps.org/supplemental/10.1103/PhysRevB.107.075434> for optical and structural properties and Figs. S1-S6 (UV-visible optical absorption and steady-state PL spectra, a XRD pattern, TEM and HR-TEM images along with EDX spectra, XPS spectra, PL decay characteristics, and a STM topography of undoped/manganese-doped ZnS QDs).
- [28] Y. L. Soo, Z. H. Ming, S. W. Huang, Y. H. Kao, R. N. Bhargava, and D. Gallagher, Local structures around Mn luminescent centers in Mn-doped nanocrystals of ZnS, *Phys. Rev. B* **50**, 7602 (1994).
- [29] M. Bode, Spin-polarized scanning tunnelling microscopy, *Rep. Prog. Phys.* **66**, 523 (2003).
- [30] D. Wortmann, S. Heinze, P. Kurz, G. Bihlmayer, and S. Blügel, Resolving Complex Atomic-Scale Spin Structures by Spin-Polarized Scanning Tunneling Microscopy, *Phys. Rev. Lett.* **86**, 4132 (2001).
- [31] L. Berbil-Bautista, S. Krause, M. Bode, and R. Wiesendanger, Spin-polarized scanning tunneling microscopy and spectroscopy of ferromagnetic Dy(0001)/W(110) films, *Phys. Rev. B* **76**, 064411 (2007).